Chemical Science

ROYAL SOCIETY OF CHEMISTRY

EDGE ARTICLE

View Article Online
View Journal



Cite this: DOI: 10.1039/d5sc05568g

All publication charges for this article have been paid for by the Royal Society of Chemistry

# Conformational adaptability enabled higher-order self-sorting processes in coordination cages

Minaz Parbin,[ab] Vellaiyadevan Sivalingam,[ab] Ramkumar Venkatachalam[a] and Dillip Kumar Chand *[ab]

Received 25th July 2025
Accepted 10th December 2025

DOI: 10.1039/d5sc05568g

rsc.li/chemical-science

Understanding the key role of conformational adaptability in biological processes is crucial to mimic the remarkable applications inherent to biological systems. Motivated by the efficacy of conformational adaptability, we equipped a conformationally-adaptive ligand in low-symmetry *cis*-$Pd_2L^a_2L^x_2$-type coordination cages. A family of five *cis*-$Pd_2L^a_2L^x_2$-type cages was assembled by complementary ligand pairing of a conformationally adaptable converging ligand ($L^a$-type) in combination with diverging rigid ligands ($L^x$-type) of different lengths. Integrative self-sorting of the individual cages showed that the converging ligand adapts to three distinct conformations in the $Pd_2L^a_2L^x_2$-type architecture, to accommodate $L^x$-type ligands of varying sizes. Through a series of experiments, we found a higher order, *i.e.*, 2-fold heteromeric completive self-sorting outcomes of two co-existing $Pd_2L^a_2L^x_2$-type cages, where two chosen complementary rigid ligands could induce any two different conformations of the converging ligand in the co-existing cages. Then we further pushed the intricacy and demonstrated the unprecedented 3-fold heteromeric completive self-sorting in coordination cage systems, where the conformationally-adaptive ligand adapts three distinct conformations in three co-existing $Pd_2L^a_2L^x_2$-type cages. This study paves the way for the utility of conformational adaptability to achieve switchable size, shape, and functionality in supramolecular systems toward bio-relevant applications.

## Introduction

Coordination-driven self-assembly has been one of the most convenient strategies for constructing captivating nanostructured coordination architectures with applications such as molecular recognition, drug delivery, separation, catalysis, *etc.*[1,2] Besides self-assembly, the controlled formation of well-defined coordination assemblies relies on the ability of the different components to associate together by mutual recognition, also known as self-sorting.[3] Inspired by biological systems, mixed ligated coordination cages were achieved through self-sorting using various design strategies (*e.g.*, geometric complementarity, coordination sphere engineering, endohedral-functionalization, guest-templation) that employ more than one type of ligand component.[4] A rational combination of up to four different ligands was used to selectively achieve discrete Pd(II)-based binuclear assemblies (*i.e.*, $Pd_2L^a_3L^b$, *cis*-/*trans*-$Pd_2L^a_2L^b_2$, *cis*-/*trans*-$Pd_2L^a_2L^bL^c$, and $Pd_2L^aL^bL^cL^d$-type) *via* integrative self-sorting.[5] However, in biological self-assembly, the encoded subcomponents assemble into more than one co-existing ensemble *via* orthogonal self-sorting.[6]

Recently, Clever group reported stoichiometrically controlled co-formation of two mixed ligated cages of $Pd_2L^a_2L^b_2$- and $Pd_2L^a_2L^c_2$-type, also known as 2-fold heteromeric completive self-sorting by both direct ligand assembly with Pd(II) or cage fusion reaction of the three high-symmetry homoleptic assemblies.[7] Later, we demonstrated a 2-fold heteromeric completive self-sorting outcome using a combination of two low-symmetry homoleptic cages and a high-symmetry homoleptic cage.[8]

Further, exploring increasingly-complex, higher-order self-sorting processes using coordination cages could be a formidable challenge, as it will require comprehensive pre-programming of the individual components along with interference-free interplay of multiple metal–ligand interactions.[6,9] However, we intend to develop a design strategy to demonstrate the co-formation of three distinct $Pd_2L^a_2L^x_2$-type mixed ligated assemblies (*i.e.*, $Pd_2L^a_2L^b_2$, $Pd_2L^a_2L^c_2$, and $Pd_2L^a_2L^d_2$-type, where x = b, c, and d) having a common $L^a$-type ligand. Such a higher-order self-sorting outcome, termed as "3-fold heteromeric completive self-sorting" is illustrated in Fig. 1. Designing the mutually shared ligand ($L^a$-type) is crucial for enabling such complexity in self-sorting processes. We presume that conformationally adaptable units embedded in a mutually shared ligand could enable the possibility of different co-existing conformations suitable for other complementary ligands ($L^x$-type, x = b, c, d, *etc.*) to form mixed ligated $Pd_2L^a_2L^x_2$-type cages using an adaptive shape-complementary approach.

[a]*Department of Chemistry, Indian Institute of Technology Madras, Chennai 600036, India. E-mail: dillip@zmail.iitm.ac.in*

[b]*IoE Center of Molecular Architecture, Department of Chemistry, Indian Institute of Technology Madras, Chennai 600036, India*

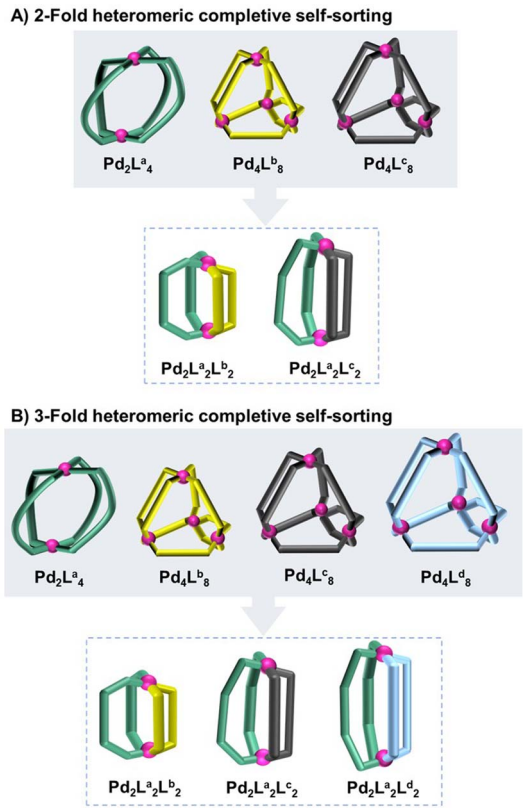


Fig. 1 (A) 2-Fold heteromeric completive self-sorting of three homoleptic assemblies into two coexisting mixed ligated assemblies. (B) 3-Fold heteromeric completive self-sorting of four homoleptic assemblies into three coexisting mixed ligated assemblies.

Though conformational adaptability plays a key role in various biological processes (such as enzymatic catalysis, allosteric signalling, ligand binding in proteins, *etc.*), achieving conformational control in synthetic supramolecular hosts requires substantial effort.[10,11] We envisaged that the conformational flexibility of amides stemming from the possible free rotation around $C_{R1}$–$C_{carbonyl}$ and $C_{R2}$–$N_{amide}$ bonds could potentially serve this purpose.[12] A significant challenge in utilizing amide-incorporated ligands for constructing mixed ligated cages would be controlling the inherently flexible nature of the ligands. However, we believe, a delicate balance between flexibility and rigidity in the ligand designs may bring the required structural diversity in mixed ligated assemblies to achieve a 3-fold heteromeric completive self-sorting outcome.

In this report, we have designed a di-amide incorporated converging bidentate ligand ($L^a$-type) and explored the conformationally adaptive trait of the ligand with a series of pillar-type diverging bidentate ligands ($L^x$-type) of appropriate lengths (Fig. 2) to construct a family of *cis*-$Pd_2L^a_2L^x_2$-type mixed ligated assemblies. The conformation of the $L^a$-type ligand (*syn–syn*, *syn–anti*, or *anti–anti*) in the formed coordination assembly is dictated by the length of the $L^x$-type diverging ligands employed for complexation. The conformational adaptability of the $L^a$-type ligand was further utilized to demonstrate the first example of a 3-fold heteromeric completive self-sorting in coordination cage systems. The three distinct coexisting binuclear assemblies ($Pd_2L^a_2L^b_2$, $Pd_2L^a_2L^c_2$, and $Pd_2L^a_2L^d_2$-type) were achieved by cage fusion of four carefully chosen homoleptic assemblies ($Pd_2L^a_4$, $Pd_4L^b_8$, $Pd_4L^c_8$, and $Pd_4L^d_8$-type), where the mutually shared $L^a$-type ligand is locked in three different conformations in the three mixed ligated cages. Further, we have also studied the conformational adaptability of three converging ligands having di-, mono-, and non-amide moieties in their backbone for constructing *cis*-$Pd_2L^a_2L^x_2$-type mixed ligated assemblies.

## Results and discussion

To study the utility of conformational adaptability in shape complementary *cis*-$Pd_2L^a_2L^x_2$-type mixed ligated cages,[5b,13] first, we designed a pair of converging bidentate ligands ($L^a$-type) **L1** (rigid) and **L2** (conformationally adaptable) (Fig. 2A). The converging ligands were designed to understand the relevance of rigidity *vs.* adaptability in the assembly of the desired mixed ligated cages, in combination with well-suited rigid diverging ligands ($L^x$-type) and Pd(II). Ligand **L2** was designed by embedding di-amide functionality in the 1,2-diphenylacetylene spacered ligand **L1**. We presume that the bidentate ligand bearing di-amide moieties (**L2**) could possibly orient in three distinct conformational states (namely *syn–syn*, *syn–anti*, or *anti–anti*) in mixed ligated $Pd_2L^a_2L^x_2$-type assembly, when paired alongside carefully designed diverging ligands ($L^x$-type, x = A–G) and Pd(II).

Due to the partial delocalization across the amide bond of **L2**, the rotation around the CO–NH bond will be constrained; however, rotation around $C_{phenyl}$–$C_{carbonyl}$ as well as $C_{pyridyl}$–$N_{amide}$ bonds could result in several possible conformations. Out of all the possible conformations of **L2**, the three chosen conformations are shown in Fig. 2B. The three conformations were selected for their potential ability to form a shape complementary *cis*-$Pd_2L^a_2L^x_2$-type assembly when paired with a suitable diverging ligand and Pd(II). Initial DFT (B3LYP/6-31g(d)) calculations revealed the approximate $N_{py}\cdots N_{py}$ distance of **L2** in different conformations to be around 9.6 Å (*syn–syn*, $\mathbf{L2}^{SS}$), 12.1 Å (*syn–anti*, $\mathbf{L2}^{SA}$) and 15.2 Å (*anti–anti*, $\mathbf{L2}^{AA}$) (Fig. 2B). In a *cis*-$Pd_2L^a_2L^x_2$-type assembly, **L2** could adapt any of the three conformations dictated by the complementary diverging ligand. Hence, we have chosen a series of pillar-type rigid ligands ($\mathbf{L^A}$–$\mathbf{L^G}$) of varied lengths ($N_{py}\cdots N_{py}$ distance ranging from around 5.6 to 16.8 Å). These ligands possess an approximate bent angle of 120°, which could potentially dictate the conformation of **L2** in the *cis*-$Pd_2L^a_2L^x_2$-type cage (Fig. 2C).[14–19] The combination of **L2** and the rigid pillar-type ligands ($\mathbf{L^A}$–$\mathbf{L^G}$) was expected to result in a library of *cis*-$Pd_2L^a_2L^x_2$-type mixed ligated cages. Also, **L1** could form *cis*-$Pd_2L^a_2L^x_2$-type assemblies when paired with a diverging ligand of appropriate length (from the series of $\mathbf{L^A}$–$\mathbf{L^G}$) and Pd(II), owing to the shape complementary nature. However, the number of *cis*-$Pd_2L^a_2L^x_2$-type assemblies and extent of adaptability will be limited due to the rigid backbone of **L1**. To achieve our objective, we synthesized the ligands, and the detailed synthetic procedure is given in the SI, see Section S2.

Initially, we explored the self-assembly of individual ligand components (**L1** and **L2**) with Pd(II). Complexation of $Pd(NO_3)_2$

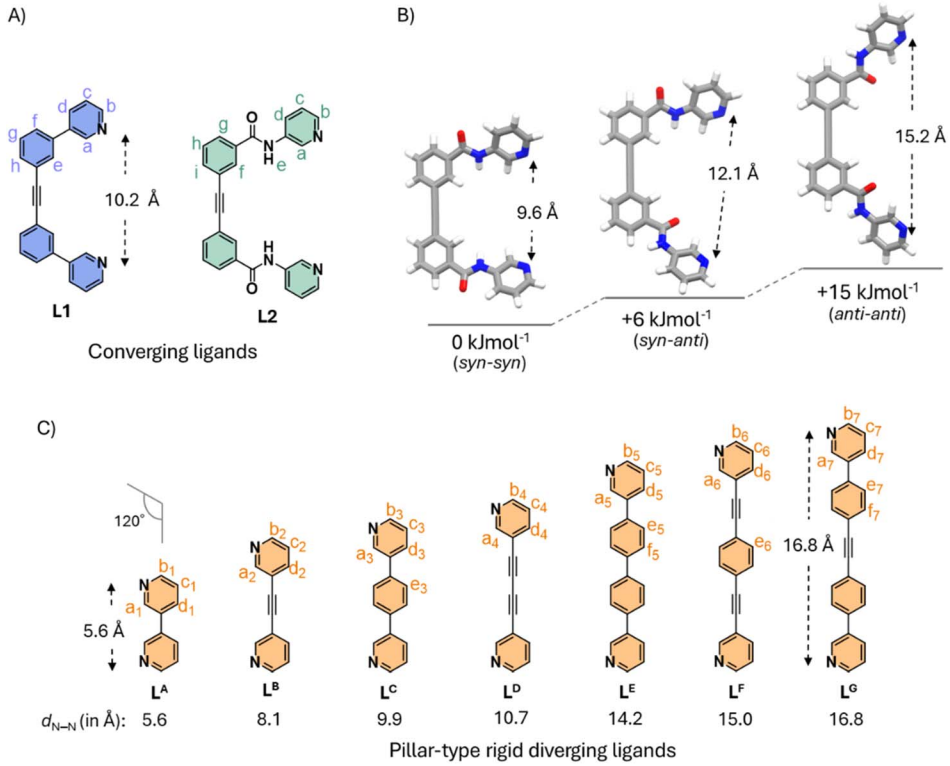


Fig. 2 Ligand designs: (A) Chemical structures of **L1** and **L2**; (B) DFT optimized structure of chosen conformations of **L2** (named as *syn–syn*, *syn–anti* and *anti–anti*) conformation, the term *syn* and *anti* are used to define the relative orientation of amide (NH) and pyridine (N) vectors); (C) Structures of ligands $L^A$–$L^G$ in increasing order of $N_{py}\cdots N_{py}$ distances (in Å). The $N_{py}\cdots N_{py}$ distances are calculated from the optimized structures (Fig. S184).

with **L1** (1 : 2 ratio) in DMSO-$d_6$ at room temperature was monitored by $^1$H NMR spectroscopy (Fig. S12). After 12 hours, a single species showing a characteristic complexation-induced downfield shift of the pyridine-αCH protons ($\Delta\delta_{\text{Complex-Ligand}}$ ($H_a$) = 0.93 ppm & $\Delta\delta_{\text{Complex-Ligand}}$ ($H_b$) = 0.76 ppm) was observed in the $^1$H NMR spectrum. Formation of the cage $[Pd_2(\mathbf{L1})_4](NO_3)_4$, $\mathbf{1}\cdot 4NO_3$ was supported based on ESI-MS data. To attain a parallel coordination vector for a $Pd_2L_4$-type assembly, the converging ligand **L1** needs to undergo twisting around the two Pd(II) centres. Hence, the formed cage was expected to be a helical $Pd_2L_4$-type assembly (Fig. S186). Likewise, the self-assembly of **L2** with Pd(II) was anticipated to result in a helical $Pd_2L_4$-type architecture (Fig. S186).[5a,13] Complexation of $Pd(NO_3)_2$ with **L2** (1 : 2 ratio) in DMSO-$d_6$ at room temperature for 12 hours led to the formation of a discrete product, as confirmed by $^1$H NMR spectroscopy (Fig. S17). ESI-MS analysis confirms the composition $[Pd_2(\mathbf{L2})_4](NO_3)_4$, $\mathbf{2}\cdot 4NO_3$ for the resultant cage assembly. Further, $^1$H–$^1$H NOE spectrum analysis of the cage showed cross-peak correlations of amide protons ($NH_e$) with outward-pointing protons $H_d$ and $H_g$ (Fig. S21), suggesting an all-(*anti–anti*) conformer of **L2** in the cage structure.

Pd(II)-based coordination complexes featuring $\mathbf{L^B}$, $\mathbf{L^C}$, $\mathbf{L^E}$, $\mathbf{L^F}$, and $\mathbf{L^G}$ have been previously reported.[16,19–21] In this work, we carried out the individual complexation of all the ligands with $Pd(NO_3)_2$ (reported cages were reproduced; see SI Section S2.4). Among the reported cases, $\mathbf{L^B}$ and $\mathbf{L^C}$ gave their respective $Pd_4L_8$ (tetrahedron)-type (*i.e.*, $\mathbf{B}\cdot 8NO_3$ and $\mathbf{C}\cdot 8NO_3$, respectively) architecture upon complexation with $Pd(NO_3)_2$.[16,20] When $\mathbf{L^A}$ was treated with $Pd(NO_3)_2$ at a 2 : 1 ratio in DMSO-$d_6$ at room temperature for 24 hours, the $^1$H NMR spectrum showed unassignable complicated signals due to the formation of a mixture of products. Complexation of $Pd(NO_3)_2$ with $\mathbf{L^D}$ at a 1 : 2 ratio in DMSO-$d_6$ at room temperature for 3 hours resulted in a well-resolved $^1$H NMR spectrum consisting of two products. The resultant assemblies are proposed to be a mixture of $Pd_4L_8$ (tetrahedron) (major) and $Pd_3L_6$ (minor)-type cages (*i.e.*, $\mathbf{D}\cdot 8NO_3$ and $\mathbf{D'}\cdot 6NO_3$. Similarly, $\mathbf{L^E}$ and $\mathbf{L^F}$ also produced a mixture of $Pd_4L_8$ (tetrahedron) (major) and $Pd_3L_6$ (minor)-type cages (*i.e.*, $\mathbf{E}\cdot 8NO_3$ and $\mathbf{E'}\cdot 6NO_3$/$\mathbf{F}\cdot 8NO_3$ and $\mathbf{F'}\cdot 6NO_3$).[16,21] However, when a longer ligand $\mathbf{L^G}$ was treated with $Pd(NO_3)_2$ (2 : 1 ratio), a single set of peaks were observed in the $^1$H NMR spectrum, suggesting the formation of a single species, a $Pd_3L_6$-type ($\mathbf{G}\cdot 6NO_3$) architecture was further confirmed by ESI-MS data analysis (Fig. S96).[19]

Next, we explored the mixed ligand complexation behavior of **L1** and **L2** when paired with a rigid diverging ligand of suitable length and Pd(II). Based on the DFT calculated structure, we presume that **L1** ($N_{py}\cdots N_{py}$ = 10.2 Å) and $\mathbf{L^B}$ ($N_{py}\cdots N_{py}$ = 8.1 Å) could be the best fit for a *cis*-$Pd_2L_2^aL_2^x$-type arrangement (Fig. S186).[22] Self-assembly of $Pd(NO_3)_2$ with **L1** and $\mathbf{L^B}$ in a 1 : 1 : 1 ratio in DMSO-$d_6$ at room temperature for 30 minutes resulted in the clean formation of a discrete cage, as demonstrated by $^1$H NMR spectroscopy. Further evidence for the formation of the

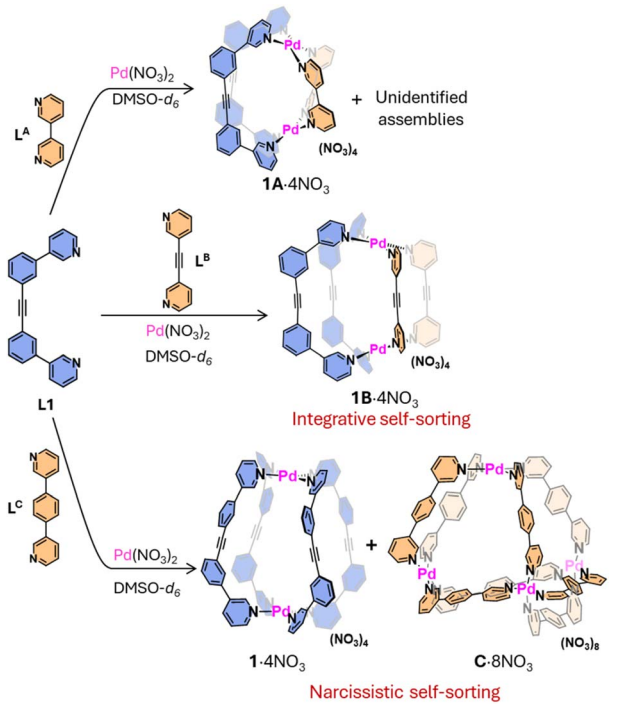


Fig. 3 Schematic representation for mixed ligand complexation of $Pd(NO_3)_2$ with L1 and $L^A$–$L^C$.

mixed ligated cage $[Pd_2(\mathbf{L1})_2(\mathbf{L^B})_2](NO_3)_4$, $\mathbf{1B}\cdot 4NO_3$ was provided by ESI-MS data, which shows isotopic peak patterns at $m/z$ = 681.09 and 433.30 corresponding to the loss of two and three $NO_3^-$ ions, respectively. Subsequently, we performed complexation of $Pd(NO_3)_2$ with **L1** and $\mathbf{L^A}$/$\mathbf{L^C}$ (shorter/longer than $\mathbf{L^B}$) (Fig. 3). Mixing $Pd(NO_3)_2$, **L1** and $\mathbf{L^A}$ in a 1 : 1 : 1 ratio in DMSO-$d_6$ showed formation of a mixture of assemblies with one dominant species in the $^1$H NMR spectrum (Fig. S31). ESI-MS data showing characteristic peak patterns for the sequential loss of $NO_3^-$ ions supported the composition of $[Pd_2(\mathbf{L1})_2(\mathbf{L^A})_2](NO_3)_4$, $\mathbf{1A}\cdot 4NO_3$. However, pairing the rigid ligand **L1** with a relatively longer ligand $\mathbf{L^C}$ and $Pd(NO_3)_2$ resulted in a mixture of homoleptic assemblies (narcissistic self-sorting), as evident from the $^1$H NMR spectrum (Fig. S44). Further employing longer ligands $\mathbf{L^D}$–$\mathbf{L^G}$ for complexation with $Pd(NO_3)_2$ and **L1** also resulted in narcissistic self-sorting (Fig. S45–S48). Integratively self-sorted *cis*-$Pd_2L_2^aL_2^x$-type assembly was only successful for the self-assembly **L1** with $\mathbf{L^B}$ and Pd(II), whereas due to the rigid backbone of **L1** and incompatible lengths of the ligand pairs, the mixed ligand assembly of **L1**, and other ligands from the series, *i.e.*, $\mathbf{L^A}$, $\mathbf{L^C}$–$\mathbf{L^G}$ was unsuccessful.

Then, we studied the adaptive self-assembly behavior of the ligand **L2** in the presence of a range of diverging ligands towards the assembly of *cis*-$Pd_2L_2^aL_2^x$-type cages. We thought $\mathbf{L^B}$ ($N_{py}\cdots N_{py}$ = 8.1 Å) would be suitable for the *syn–syn* conformation ($\mathbf{L2}^{SS}$, $N_{py}\cdots N_{py}$ = 9.6 Å). Upon treating **L2** and $\mathbf{L^B}$ with $Pd(NO_3)_2$ in a 1 : 1 : 1 ratio in DMSO-$d_6$ at room temperature for 30 minutes, the $^1$H NMR spectrum showed a single set of signals for the formation of a discrete species. The spectrum showed the characteristic complexation-induced downfield shift in the position of the inwards pointed pyridine-$\alpha CH_{IN}$ of both the ligands ($\Delta\delta_{Complex\text{-}Ligand}$ ($H_a$) = 0.51 ppm & $\Delta\delta_{Complex\text{-}Ligand}$ ($H_{a2}$) = 1.41 ppm for **L2** and $\mathbf{L^B}$ respectively) (Fig. 4B(iii)). The formation of complex $[Pd_2(\mathbf{L2})_2(\mathbf{L^B})_2](NO_3)_4$, $\mathbf{2B}\cdot 4NO_3$ was further investigated by ESI-MS data analysis, where isotopic peak patterns at $m/z$ = 490.73 and 352.55 was observed for the loss of three and four $NO_3^-$ ions, respectively. Further, a single band in the $^1$H DOSY spectrum confirmed that all the protons correspond to a single species in the solution with a diffusion coefficient of 1.21 × $10^{-10}$ $m^2$ $s^{-1}$ (Fig. S118).

To investigate the conformationally adaptive nature of ligand **L2**, we performed its complexation with the next ligand in the series $\mathbf{L^C}$ ($N_{py}\cdots N_{py}$ = 9.9 Å) and $Pd(NO_3)_2$ at a 1 : 1 : 1 ratio in DMSO-$d_6$. After 30 minutes, the $^1$H NMR spectrum indicated the formation of a discrete product corresponding to cage $[Pd_2(\mathbf{L2})_2(\mathbf{L^C})_2](NO_3)_4$, $\mathbf{2C}\cdot 4NO_3$ where the pyridine–$\alpha CH_{IN}$ showed complexation-induced downfield shift ($\Delta\delta_{Complex\text{-}Ligand}$ ($H_a$) = 0.98 ppm & $\Delta\delta_{Complex\text{-}Ligand}$ ($H_{a3}$) = 1.46 ppm for **L2** and $\mathbf{L^C}$, respectively) for both the ligands (Fig. 4B(iv)). We presume $\mathbf{L^C}$ might be slightly longer to fit the *syn–syn* conformation of **L2** in the *cis*-$Pd_2L_2^aL_2^x$-type cage structure. Thus, **L2** might have adapted *syn–anti* conformation ($\mathbf{L2}^{SA}$) during the self-assembly process to form cage $\mathbf{2C}\cdot 4NO_3$ selectively. To further test our hypothesis for the conformational adaptability of **L2**, we performed complexation of $Pd(NO_3)_2$ with **L2** and $\mathbf{L^D}$ ($N_{py}\cdots N_{py}$ = 10.7 Å) (1 : 1 : 1 ratio) in DMSO-$d_6$. After stirring the reaction at room temperature for 30 minutes, a discrete assembly was observed in the $^1$H NMR spectrum (Fig. 4B(v)). The composition of the formed product was found to be $[Pd_2(\mathbf{L2})_2(\mathbf{L^D})_2](NO_3)_4$, $\mathbf{2D}\cdot 4NO_3$ from ESI-MS data analysis. The facile formation of complex $\mathbf{2D}\cdot 4NO_3$ confirms the ability of **L2** to adapt to a different conformation to form an entropically more favourable mixed ligated cage.

Having found an adaptive ligand capable of switching its conformation to adopt a length suitable for fitting a complementary ligand in a $Pd_2L_2^aL_2^x$-type cage, we next decided to attempt the complexation of $Pd(NO_3)_2$ with **L2** and $\mathbf{L^E}$ ($N_{py}\cdots N_{py}$ = 14.2 Å) or $\mathbf{L^F}$ ($N_{py}\cdots N_{py}$ = 15.0 Å). A clean formation of the cage $[Pd_2(\mathbf{L2})_2(\mathbf{L^E})_2](NO_3)_4$, $\mathbf{2E}\cdot 4NO_3$ and $[Pd_2(\mathbf{L2})_2(\mathbf{L^F})_2](NO_3)_4$, $\mathbf{2F}\cdot 4NO_3$ was obtained *via* self-assembly of **L2** with $\mathbf{L^E}$/$\mathbf{L^F}$ and $Pd(NO_3)_2$ respectively (Fig. 4B(vi and vii)). The formed mixed ligated assemblies were characterized by 1D and 2D NMR spectroscopy techniques and ESI-MS data. Based on the $N_{py}\cdots N_{py}$ distances of $\mathbf{L^E}$ and $\mathbf{L^F}$, we could infer that the **L2** is likely to be present in the *anti–anti* conformation ($\mathbf{L2}^{AA}$). To examine the extent of conformational adaptability of **L2** for the formation of $Pd_2L_2^aL_2^x$-type assembly, we tried the complexation with the shortest/longest ligand in the chosen series, *i.e.*, $\mathbf{L^A}$ ($N_{py}\cdots N_{py}$ = 5.6 Å) and $\mathbf{L^G}$ ($N_{py}\cdots N_{py}$ = 16.8 Å). Expectedly, both ligands were found to yield either a narcissistic self-sorting outcome or a mixture of unidentified assemblies.

The comparative $^1$H NMR spectral analysis of all five *cis*-$Pd_2L_2^aL_2^x$-type cages, $\mathbf{2B}\cdot 4NO_3$–$\mathbf{2F}\cdot 4NO_3$, showed distinctive complexation-induced chemical shift changes ($\Delta\delta_{Complex\text{-}Ligand}$) for $H_a$ and $H_d$ (Fig. 4B). While the $^1$H NMR spectrum of $\mathbf{2B}\cdot 4NO_3$ exhibited $\Delta\delta_{Complex\text{-}Ligand}$ for $H_a$ about 0.51 ppm (downfield shift), the cages $\mathbf{2C}\cdot 4NO_3$ and $\mathbf{2D}\cdot 4NO_3$ displayed even higher $\Delta\delta_{Complex\text{-}Ligand}$ for $H_a$ (0.98 ppm and 1.00 ppm). However, for

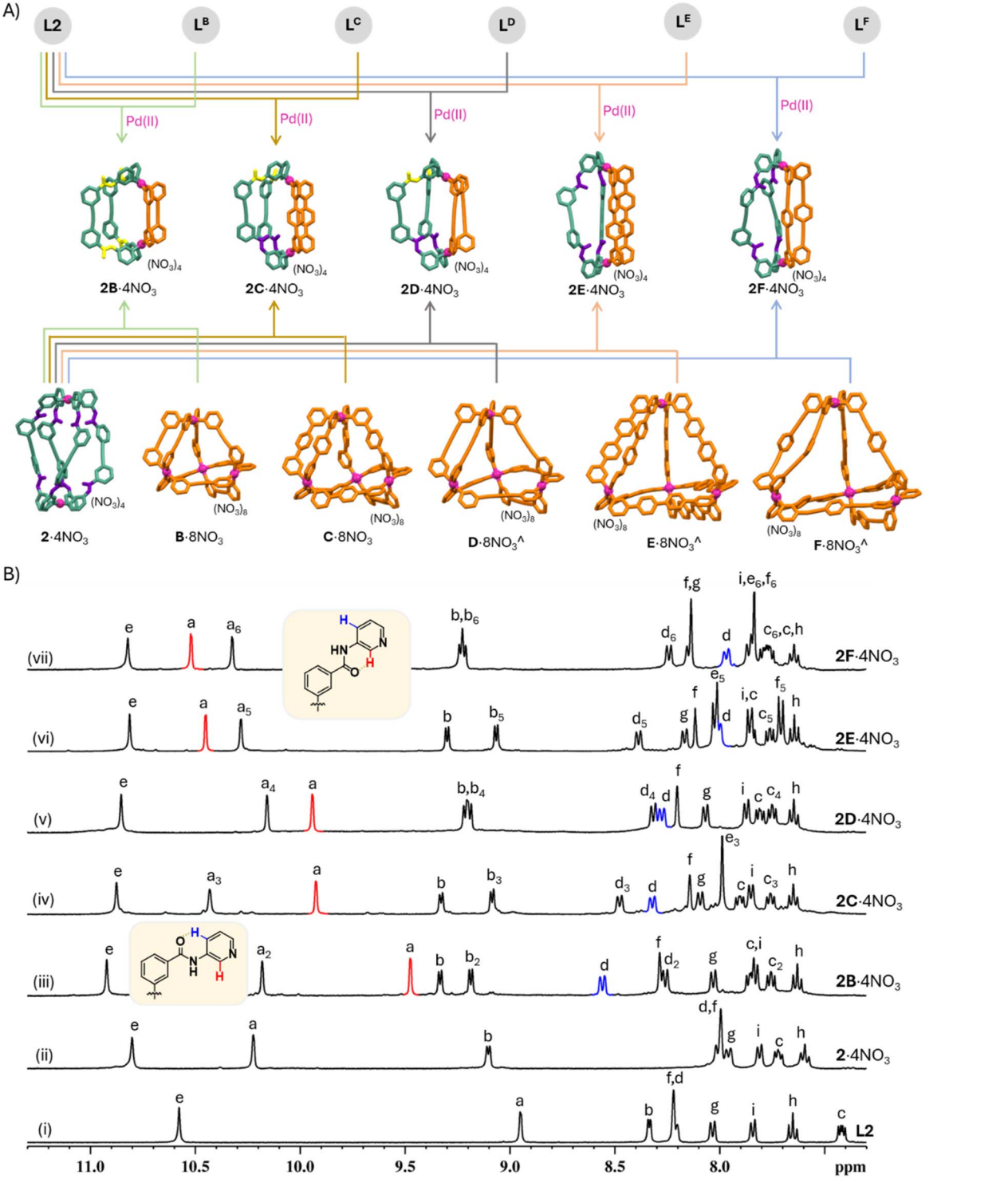


Fig. 4 (A) Self-assembly of a conformationally adaptive ligand to form a series of $Pd_2L^a_2L^x_2$-type mixed ligated cages. Energy-minimized structures of the cationic complexes were used to represent the cages. ^only the major product is shown; (B) Partial $^1$H NMR spectra (400 MHz, 298 K, DMSO-$d_6$) of (i) **L2**; (ii) $[Pd_2(L2)_4](NO_3)_4$ , **2**·$4NO_3$; (iii) $[Pd_2(L2)_2(L^B)_2](NO_3)_4$, **2B**·$4NO_3$; (iv) $[Pd_2(L2)_2(L^C)_2](NO_3)_4$, **2C**·$4NO_3$; (v) $[Pd_2(L2)_2(L^D)_2](NO_3)_4$, **2D**·$4NO_3$; (vi) $[Pd_2(L2)_2(L^E)_2](NO_3)_4$, **2E**·$4NO_3$; vii) $[Pd_2(L2)_2(L^F)_2](NO_3)_4$, **2F**·$4NO_3$.

the cages **2E**·$4NO_3$ and **2F**·$4NO_3$, we found more pronounced $\Delta\delta_{Complex\text{-}Ligand}$ for $H_a$ (1.52 ppm and 1.58 ppm). Likewise, a similar observation was found for the proton $H_d$, which showed gradual upfield shifts from **2B**·$4NO_3$ to **2F**·$4NO_3$. This distinctive chemical shift change may be due to the intramolecular hydrogen bonding between $H_a$/$H_d$ and carbonyl oxygen. As the conformational switching progressively changes from *syn–syn* to *anti–anti via syn–anti* conformation, $H_a$/$H_d$ could potentially move closer/away from C=O, respectively.

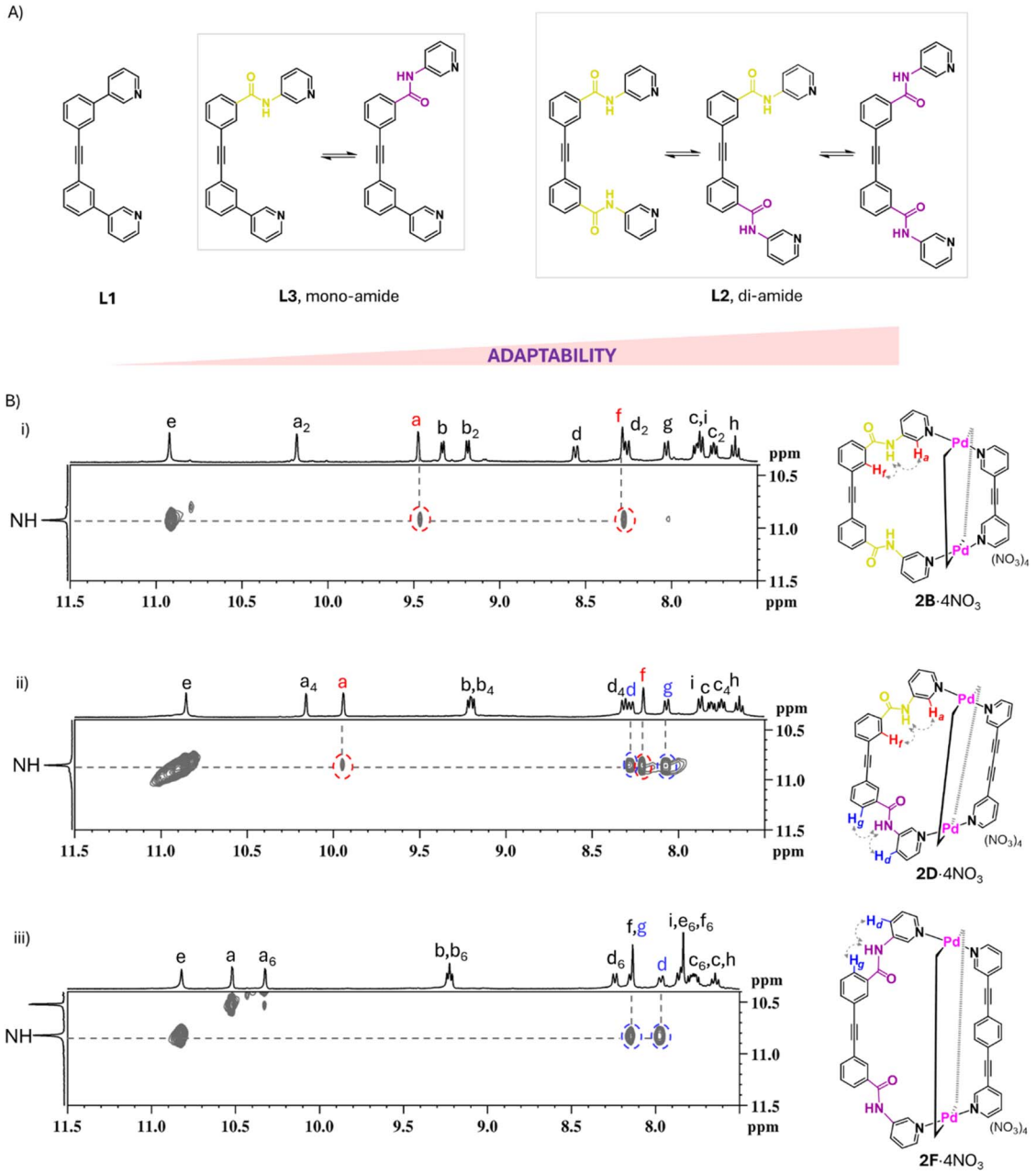


Fig. 5 (A) Conformational adaptability (with the chosen distinct conformations) trend for the ligands **L1**, **L3** (mono-amide) and **L2** (di-amide) towards the construction of *cis*-$Pd_2L_2^aL_2^x$-type mixed ligated assemblies; (B) expanded $^1H-^1H$ NOE spectra (400 MHz, 298 K, DMSO-$d_6$) showing intra-ligand cross peaks for strong correlation of the amide protons (N–$H_e$) with inward (*syn*) or outward (*anti*) pointing protons of the pyridine and phenyl groups in (i) **2B**·$4NO_3$; (ii) **2D**·$4NO_3$ and (iii) **2F**·$4NO_3$, respectively.

After successfully achieving a series of cages **2B**·$4NO_3$–**2F**·$4NO_3$ through integrative self-sorting of individual ligand components and Pd(II) using an adaptive shape-complementary approach, we were curious to inspect whether the self-assembled products are pathway-dependent or at the thermodynamic minimum. Hence, we performed the cage-to-cage transformations from the corresponding homoleptic assemblies. Mixing 2 equiv. of **2**·$4NO_3$ with 1 equiv. of corresponding homoleptic assemblies of $\mathbf{L^x}$ ($\mathbf{x}$ = **B**–**F**), *i.e.*, **B**·$8NO_3$–**F**·$8NO_3$ ($Pd_4L_8$-type cages **D**·$8NO_3$, **E**·$8NO_3$ and **F**·$8NO_3$ exist along with the $Pd_3L_6$-type cages **D′**·$6NO_3$, **E′**·$6NO_3$ and **F′**·$6NO_3$), individually in DMSO-$d_6$, resulted in the mixed ligated assembly **2X**·$4NO_3$ under thermodynamic control (Fig. 4A). The robustness of the mixed ligated cage **2B**·$4NO_3$–**2F**·$4NO_3$ was further demonstrated by concentration variation studies (SI Section S8 and Fig. S151–S155).

Thereafter, we were curious to inspect the conformational preference of ligand **L2** in the $Pd_2L_2^aL_2^x$-type cage assemblies. For this purpose, we performed ligand exchange reactions, in which to a chosen mixed ligated complex, a calculated amount of another ligand (from the series $\mathbf{L^B}$–$\mathbf{L^F}$) was added. In some cases, the bound ligand has been replaced partially or entirely

by the incoming ligand (SI Section S9, Scheme S32 and Fig. S156–S175). Based on these experiments, the relative ligand selectivity of **L2** to form mixed ligated cages was found to be $\mathbf{L^E} > \mathbf{L^C} > \mathbf{L^F} > \mathbf{L^B} \simeq \mathbf{L^D}$. Based on the electrostatic potential map analysis of the ligands $\mathbf{L^B}$–$\mathbf{L^F}$, we presume this outcome could possibly be due to the basicity of the rigid complementary ligands rather than the conformation of the **L2** (Fig. S185).

The striking difference in the adaptability of **L1** and **L2** to self-assemble into *cis*-$Pd_2L_2^aL_2^x$-type cages stems from the embedded amide moieties in **L2**. When **L1** was paired with a set of diverging ligands ($\mathbf{L^x}$, $N_{py}\cdots N_{py}$ = 5.6–16.8 Å), an absolute integrative self-sorted product was obtained only for the case of $\mathbf{L^B}$. Whereas integrative self-sorting of **L2** was successful for a series of five ligands, *i.e.*, $\mathbf{L^B}$–$\mathbf{L^F}$ ($N_{py}\cdots N_{py}$ = 8.1–15.0 Å), resulting in a family of five *cis*-$Pd_2L_2^aL_2^x$-type assemblies ($\mathbf{2B}\cdot 4NO_3$–$\mathbf{2F}\cdot 4NO_3$). Thus, we were curious to study the adaptability of a converging ligand with a single amide moiety embedded. Hence, we chose a mono-amide functionalized ligand **L3**, for the complexation with $\mathbf{L^A}$–$\mathbf{L^G}$.

In our previous report,[8] we utilized **L3** (a structurally-constrained ligand) along with suitable symmetrical/unsymmetrical diverging ligands and Pd(II) to develop two highly anisotropic binuclear mixed ligated cages. However, the conformational adaptability of **L3** was unexplored. To investigate the full extent of adaptability of **L3** in the presence of suitable diverging ligands, we attempted the complexation of $Pd(NO_3)_2$ with **L3** and $\mathbf{L^A}$–$\mathbf{L^G}$. We previously obtained the mixed ligated cage, *i.e.*, $[Pd_2(\mathbf{L3})_2(\mathbf{L^B})_2](NO_3)_4$, $\mathbf{3B}\cdot 4NO_3$ as the minor product upon complexation of **L3** and $\mathbf{L^B}$ with Pd(II). Whereas in the case of $\mathbf{L^C}$, an exclusive formation of $[Pd_2(\mathbf{L3})_2(\mathbf{L^C})_2](NO_3)_4$, $\mathbf{3C}\cdot 4NO_3$ was achieved. Among the newly attempted cases (*i.e.*, $\mathbf{L^A}$, $\mathbf{L^D}$–$\mathbf{L^G}$), we successfully obtained discrete mixed ligated assembly $[Pd_2(\mathbf{L3})_2(\mathbf{L^D})_2]](NO_3)_4$, $\mathbf{3D}\cdot 4NO_3$ from the combination of **L3**, $\mathbf{L^D}$ and $Pd(NO_3)_2$, as indicated by $^1$H NMR spectroscopy and ESI-MS data (Fig. S82 and S112). Since **L3** is unsymmetrical in nature, the mixed ligated cage was obtained as an isomeric mixture of two possible isomers of cage $\mathbf{3D}\cdot 4NO_3$ (Fig. S186). For all the other cases, the mixed ligated assembly of **L3** and the diverging ligands ($\mathbf{L^A}$, $\mathbf{L^E}$–$\mathbf{L^G}$) were unsuccessful. So, the mono-amide ligand **L3** can adapt to two different diverging ligands ($\mathbf{L^C}$ and $\mathbf{L^D}$), producing the desired *cis*-$Pd_2L_2^aL_2^x$-type cages (where **L3** is in *anti*-conformation in the cage structures, Fig. S85); while the rigid **L1** yielded only one *cis*-$Pd_2L_2^aL_2^x$-type cage through integrative self-sorting. Hence, we infer that the conformational adaptability of **L3** falls somewhere between **L1** and **L2**. This showcases that the extent of conformational adaptability is proportional to the number of embedded amide units in the ligand backbone (Fig. 5A).

In the $Pd_2L_2^aL_2^x$-type assembly, the identical ligands coordinate to the Pd(II) centres in a *cis* fashion, where **L2** can adapt to any of the three conformations such as *syn–syn* ($\mathbf{L2}^{SS}$), *syn–anti* ($\mathbf{L2}^{SA}$) and *anti–anti* ($\mathbf{L2}^{AA}$) in the cage structure. Earlier, we postulated the existence of three conformations based on the complexation-induced chemical shift changes in protons $H_a$ and $H_d$, presumably due to possible intramolecular hydrogen bonding interactions with carbonyl oxygen (Fig. 4B). Next, we used $^1$H–$^1$H NOE spectroscopy to verify the existing conformations of **L2** in all five mixed-ligated cages. In the NOE spectrum of $\mathbf{2B}\cdot 4NO_3$, the amide proton (N–$H_e$) shows strong cross-peak correlations with $H_a$ and $H_f$, indicating that the **L2** is present in a *syn–syn* conformation ($\mathbf{L2}^{SS}$) (Fig. 5B(i)). Similarly, we found NOE correlations for the amide protons (N–$H_e$) of $\mathbf{2E}\cdot 4NO_3$ and $\mathbf{2F}\cdot 4NO_3$ with $H_d$ and $H_g$, no correlations were found with $H_a$/$H_f$, indicating the ligand conformation to be *anti–anti* ($\mathbf{L2}^{AA}$) in the cage (Fig. 5B(iii) and S73). Understandably, the cages $\mathbf{2C}\cdot 4NO_3$ and $\mathbf{2D}\cdot 4NO_3$ showed multiple NOE correlations for the amide N–$H_e$ with $H_a$, $H_d$, $H_f$, and $H_g$ suggesting a *syn–anti* ($\mathbf{L2}^{SA}$) conformation of **L2** in the cage (Fig. 5-B(ii) and S60). In addition to the intra-ligand contacts, the NOE spectrum of all the cages also showed several cross-peaks for the inter-ligand through-space contacts between **L2** and $\mathbf{L^x}$ (x = **B**–**F**).

The *syn–syn* ($\mathbf{L2}^{SS}$) and *anti–anti* ($\mathbf{L2}^{AA}$) conformation of **L2** in $\mathbf{2B}\cdot 4NO_3$ and $\mathbf{2E}\cdot 4NO_3$/$\mathbf{2F}\cdot 4NO_3$ contributes to the overall higher symmetry of the cages. On the other hand, though the *syn–anti* ($\mathbf{L2}^{SA}$) conformation of **L2** in $\mathbf{2C}\cdot 4NO_3$ and $\mathbf{2D}\cdot 4NO_3$

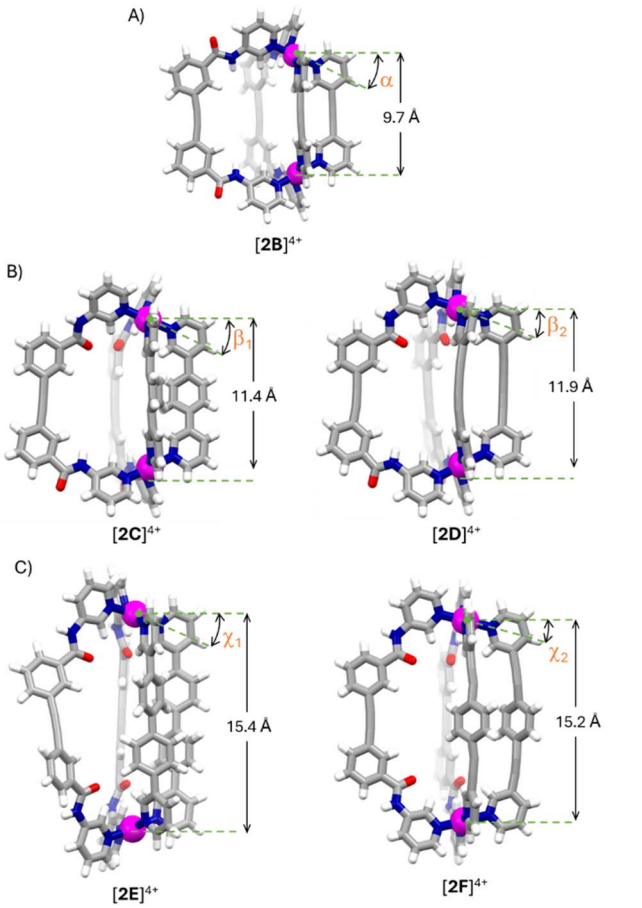


Fig. 6 (A) DFT optimized structure of $[\mathbf{2B}]^{4+}$ showing *syn–syn* conformation of **L2**; (B) SC-XRD structure of $[\mathbf{2C}]^{4+}$ and $[\mathbf{2D}]^{4+}$ showing *syn–anti* conformation of **L2**; (C) DFT optimized structure of $[\mathbf{2E}]^{4+}$ (left) and SC-XRD structure of $[\mathbf{2F}]^{4+}$(right) showing *anti–anti* conformation of **L2**. $\alpha$ = 38°; $\beta_1$ = 35°; $\beta_2$ = 32°; $\chi_1$ = 25°; $\chi_2$ = 19°. Angle $\alpha$, $\beta_1$, $\beta_2$, $\chi_1$ and $\chi_2$ represent the angle of deviation from the parallel $Pd(N_{py})_4$ planes seen in typical $Pd_2L_4^a$-type cages. Solvents and counteranions are not shown for clarity.

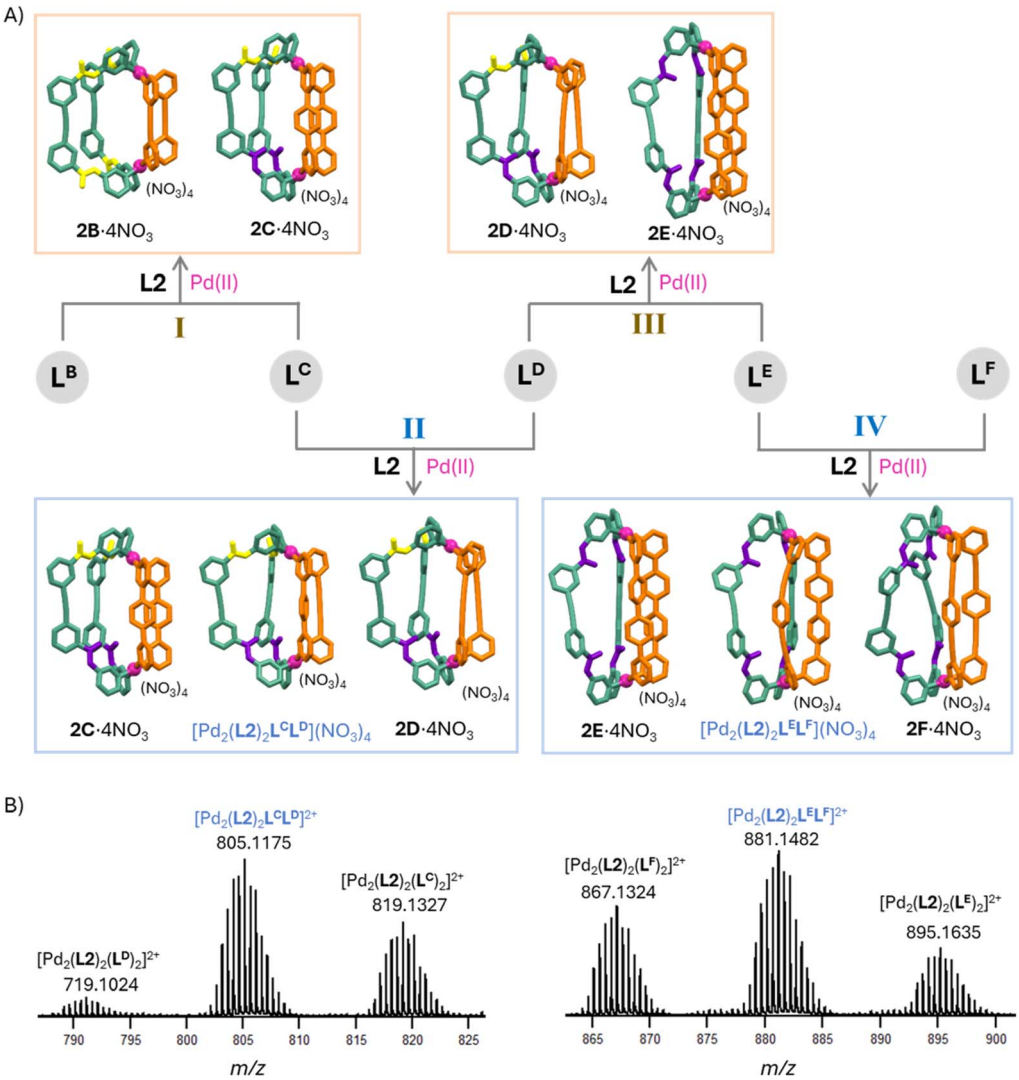


Fig. 7 (A) Selected self-sorting scenarios for the self-assembly of three ligand components with Pd(II). I and III: 2-fold heteromeric completive self-sorting; II and IV: mixed self-sorting; (B) partial ESI-MS for self-sorting scenarios in case II and IV showing mixed self-sorting products.

could lower the symmetry of the cage, we obtained a single set of signals in the $^1$H NMR spectrum, presumably due to the fast exchange between the conformations at room temperature. To restrict the ligand conformation in the cage assembly, we attempted a variable temperature NMR study (lowering the temperature up to −30 °C) using **2C**·4$BF_4$ and **2D**·4$BF_4$ in $CD_3CN$. However, we could not observe any significant splitting of the $^1$H NMR signals, suggesting the existence of fast exchange process even at −30 °C (Fig. S176 and S180). Further, the two units of **L2** in cages **2C**·4$NO_3$ and **2D**·4$NO_3$ can have either a parallel/antiparallel arrangement in the $Pd_2L^a_2L^x_2$-type-structure (Fig. S187 and S188). DFT calculation of the two possible isomers at the B3LYP/LanL2DZ, 6-31G(d) level in gas and implicit solvent (DMSO) phase suggested a lower energy for isomer-I, *i.e.*, parallel arrangement of **L2** in both the cages (SI Section S11, Table S1 and S2).

To further corroborate the conformational control in five *cis*-$Pd_2L^a_2L^x_2$-type cages, $[Pd_2(\mathbf{L2})_2(\mathbf{L}^x)_2]^{4+}$ by single crystal X-ray diffraction (SC-XRD) analysis, concerted efforts were made to crystallize the cages. We used different solvents and solvent mixtures as well as varied the counteranions. After numerous attempts, we could get crystal data suitable for SC-XRD analysis of $[\mathbf{2C}]^{4+}$ and $[\mathbf{2D}]^{4+}$ with $NO_3^-$ as counteranion by vapour diffusion of benzene : acetonitrile and toluene : *t*-butanol in DMSO solution of **2C**·4$NO_3$/**2D**·4$NO_3$, respectively. SC-XRD analysis confirmed *syn–anti* conformation of **L2** in both the cage structures (Fig. 6). Subsequently, we collected the crystal data for $[\mathbf{2F}]^{4+}$ with $BF_4^-$ as counteranion. The single crystals were obtained by vapour diffusion of THF in a mixture of DMSO : $CH_3CN$ (2 : 1) solution of **2F**·4$BF_4$. Structural analysis reiterated the existence of **L2** in *anti–anti* conformation in $[\mathbf{2F}]^{4+}$ (Fig. 6C). In cages $[\mathbf{2B}]^{4+}$–$[\mathbf{2F}]^{4+}$, the angle of intersection of the $Pd(N_{py})_4$ planes (usually parallel for typical $Pd_2L^a_4$-type cages) gradually decreased when we progressively increased the length of rigid complementary ligands.

We successfully introduced conformational adaptability in *cis*-$Pd_2L^a_2L^x_2$-type systems with embedded amide moiety in $L^a$-type ligand and suitable rigid diverging ligands ($L^x$-type), which

could dictate the requisite conformation of $L^a$ in the cage. The control over the choice of conformations based on the length of rigid diverging ligands opens the possibility of exploring the higher-order self-sorting processes using $Pd_2L^a_2L^x_2$-type cages. We presume that three distinct conformations of **L2** (where **L2** can be used as a common ligand) could enable up to an unprecedented 3-fold heteromeric completive self-sorting (*i.e.*, three co-existing mixed ligated assemblies) in coordination cages.

We set out to explore the conformationally adaptive nature of ligand **L2** to demonstrate the self-assembly of three different ligands and Pd(II), targeting the assembly of two co-existing $Pd_2L^a_2L^x_2$-type cages, also known as 2-fold heteromeric completive self-sorting.[6,7] In the co-existing mixed ligated assemblies, we take the conformationally adaptive **L2** as a common ligand, while we use the combination of any two rigid ligands from a set of five ligands, $\mathbf{L^B}$–$\mathbf{L^F}$. For all the experiments, we treated $Pd(NO_3)_2$ with **L2** and two chosen ligands amongst $\mathbf{L^B}$–$\mathbf{L^F}$ in a 2 : 2 : 1 : 1 ratio in DMSO-$d_6$ and stirred at room temperature. In the cases where 2 consecutive ligands (*i.e.*, $\mathbf{L^B:L^C}$, $\mathbf{L^C:L^D}$, $\mathbf{L^D:L^E}$ and $\mathbf{L^E:L^F}$) were selected alongside **L2** and $Pd(NO_3)_2$ (Fig. 7A), we observed two different scenarios: (i) 2-fold heteromeric completive self-sorting outcome for the cases **I** and **III**, where a mixture of co-existing mixed-ligated cages (**2B**·$4NO_3$ + **2C**·$4NO_3$ and **2D**·$4NO_3$ + **2E**·$4NO_3$, respectively) was observed; (ii) mixed self-sorting (both integrative and heteromeirc) outcome for the cases **II** and **IV**, where we observed an additional trileptic mixed-ligated assembly[5c,d] ($[Pd_2(\mathbf{L2})_2\mathbf{L^C}\mathbf{L^D}](NO_3)_4$ and $[Pd_2(\mathbf{L2})_2\mathbf{L^E}\mathbf{L^F}](NO_3)_4$, respectively), along with heteromeric products (**2C**·$4NO_3$ + **2D**·$4NO_3$ and **2E**·$4NO_3$ + **2F**·$4NO_3$) (Fig. S125, S129, S132 and S134). Also, in case **II** the trileptic cage $[Pd_2(\mathbf{L2})_2\mathbf{L^C}\mathbf{L^D}](NO_3)_4$ was observed as the dominating species in the mixture of assemblies. ESI-MS analysis for case **II** confirmed the existence of three co-existing assemblies, **2C**·$4NO_3$, **2D**·$4NO_3$ and $[Pd_2(\mathbf{L2})_2\mathbf{L^C}\mathbf{L^D}](NO_3)_4$. Likewise, a combination of **2E**·$4NO_3$, **2F**·$4NO_3$ and $[Pd_2(\mathbf{L2})_2\mathbf{L^E}\mathbf{L^F}](NO_3)_4$ was supported by ESI-MS data for case **IV** (Fig. 7B). However, all the other diverging ligand combinations (*i.e.*, $\mathbf{L^B:L^D}$, $\mathbf{L^B:L^E}$, $\mathbf{L^B:L^F}$, $\mathbf{L^C:L^E}$, $\mathbf{L^C:L^F}$ and $\mathbf{L^D:L^F}$) apart from the cases **I**–**IV**, displayed 2-fold heteromeric completive self-sorting outcome. So, it is understandable that the heteromeric assembly using two different diverging ligands together with **L2** and $Pd(NO_3)_2$ yielded a 2-fold heteromeric completive self-sorting outcome, where the two diverging ligands could induce two different

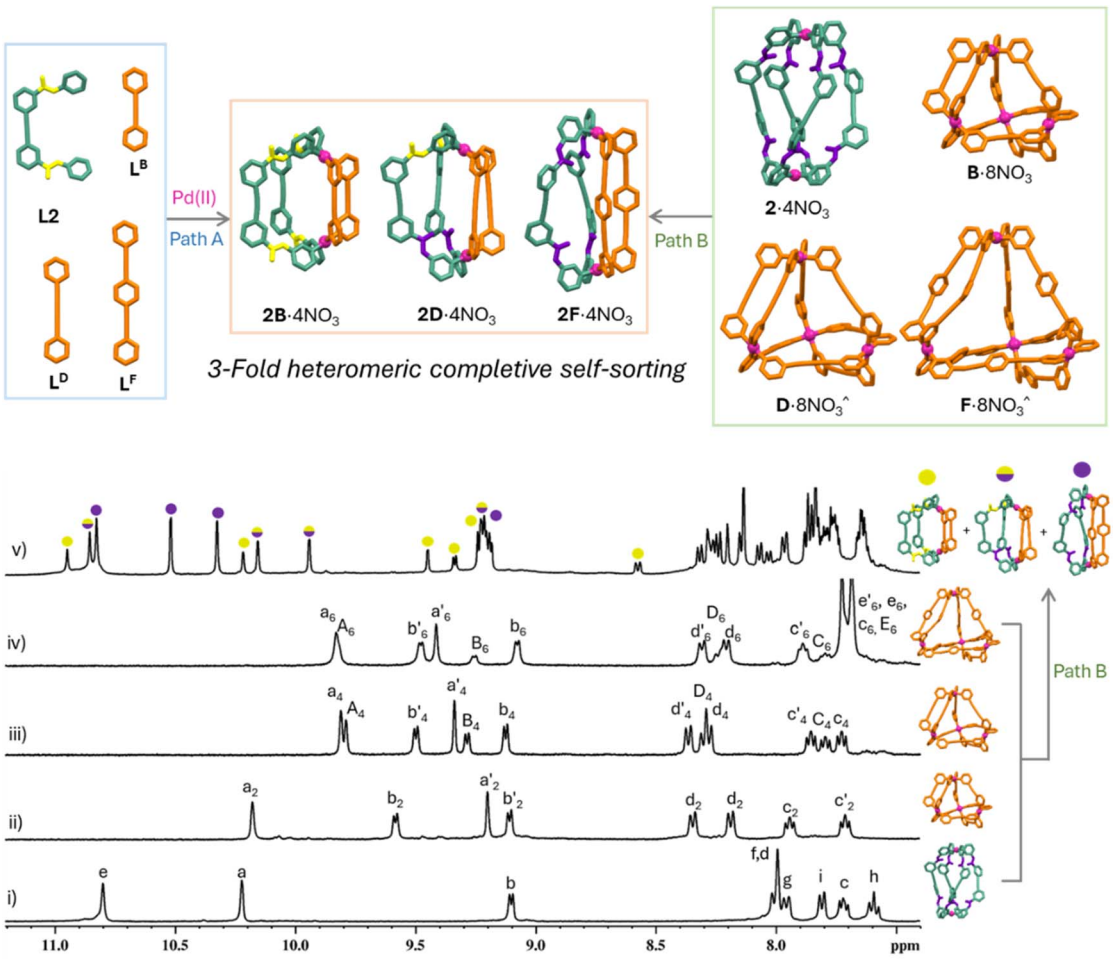


Fig. 8 3-Fold heteromeric completive self-sorting showing co-existence of three different $Pd_2L^a_2L^x_2$-type assemblies; Partial $^1H$ NMR spectra (400 MHz, 298 K, DMSO-$d_6$) of (i) **2**·$4NO_3$; (ii) **B**·$8NO_3$; (iii) **D**·$8NO_3$ (Major product) + **D′**·$6NO_3$; (iv) **F**·$8NO_3$ (Major product) + **F′**·$6NO_3$; (v) co-existing mixture of **2B**·$4NO_3$, **2D**·$4NO_3$ and **2F**·$4NO_3$.

conformations of **L2**. On the other hand, when two different diverging ligands that can induce the same conformations produce mixed self-sorting (a combination of integrative and heteromeric) outcomes. A similar self-sorting outcome was observed for cage fusion reaction (case **I–IV**) of the three homoleptic assemblies, *i.e.*, **2**·4$NO_3$ and the two chosen **X**·8$NO_3$ (**X** = **B–F**). The $^1$H NMR spectra of all the cage mixtures obtained through 2-fold heteromeric completive self-sorting are comparable to that of the respective mixed-ligated $Pd_2L_2^aL_2^x$-type cages (Fig. S125–S134).

Next, we intend to extend the self-sorting processes to a more intricate level, *i.e.*, 3-fold heteromeric completive self-sorting. Achieving three discrete co-existing mixed-ligated assemblies *via* the self-assembly of four distinct ligands could be a fascinating study. We deduced that using the diverging ligand pairs inducing two different conformations in **L2** is essential for attaining orthogonality in the coordination cage systems to achieve 2-fold heteromeric completive self-sorting. Hence, we decided to pick a mix of three diverging ligands that induce three distinct conformations of **L2** (*i.e.*, $\mathbf{L2}^{SS}$, $\mathbf{L2}^{SA}$ and $\mathbf{L2}^{AA}$) to achieve 3-fold heteromeric completive self-sorting. Firstly, we have chosen diverging ligands $\mathbf{L}^{\mathbf{B}}$, $\mathbf{L}^{\mathbf{D}}$ and $\mathbf{L}^{\mathbf{F}}$, such that **L2** would adapt to $\mathbf{L2}^{SS}$, $\mathbf{L2}^{SA}$ and $\mathbf{L2}^{AA}$ conformations in their respective mixed ligated cages. A mixture of **L2**, $\mathbf{L}^{\mathbf{B}}$, $\mathbf{L}^{\mathbf{D}}$, $\mathbf{L}^{\mathbf{F}}$ and $Pd(NO_3)_2$ (3 : 1 : 1 : 1 : 3) in DMSO-$d_6$ was stirred at room temperature for 12 hours (path A). Very interestingly, the $^1$H NMR spectrum showed clean formation of three different $Pd_2L_2^aL_2^x$-type assemblies, **2B**·4$NO_3$, **2D**·4$NO_3$ and **2F**·4$NO_3$ co-existing in the solution (Fig. S142). Here, the three different mixed-ligated assemblies share a common ligand (**L2**). However, they differ in the relative orientation of the amide moiety in the cage structures, where the ligand **L2** is locked in *syn–syn*, *syn–anti* and *anti–anti* conformations. Alternatively, the cage fusion of the four high-symmetry homoleptic assemblies **2**·4$NO_3$, **B**·8$NO_3$, **D**·8$NO_3$ and **F**·8$NO_3$ (both **D**·8$NO_3$ and **F**·8$NO_3$ exist alongside a minor product ($Pd_3L_6$)) also resulted in the simultaneous formation of three low-symmetry mixed ligated assemblies (path B) representing the 3-fold heteromeric completive self-sorting as shown in Fig. 8. Though the system involves simultaneous utilization of multiple metal–ligand interactions, full orthogonality within the $Pd_2L_2^aL_2^x$-type cages was achieved by geometric complementarity and conformational adaptability of **L2** in the presence of other rigid diverging ligands ($\mathbf{L}^{\mathbf{x}}$). A similar 3-fold heteromeric self-sorting process was also observed for the other combinations of the diverging ligands ($\mathbf{L}^{\mathbf{B}}$ : $\mathbf{L}^{\mathbf{C}}$ : $\mathbf{L}^{\mathbf{F}}$, $\mathbf{L}^{\mathbf{B}}$ : $\mathbf{L}^{\mathbf{C}}$ : $\mathbf{L}^{\mathbf{E}}$ and $\mathbf{L}^{\mathbf{B}}$ : $\mathbf{L}^{\mathbf{D}}$ : $\mathbf{L}^{\mathbf{E}}$) with **L2** and $Pd(NO_3)_2$. In all the cases, the $^1$H NMR spectrum showed clean formation of the desired co-existing mixed ligated assemblies (Fig. S139–S141).

## Conclusions

In summary, we have demonstrated a substantial change in the mixed ligand complexation behavior of a converging ligand by incorporating di-amide functionality on its backbone. While **L1** undergoes absolute integrative self-sorting with only one ligand from a series of diverging ligands ($\mathbf{L}^{\mathbf{A}}$–$\mathbf{L}^{\mathbf{G}}$) to form a *cis*-$Pd_2L_2^aL_2^x$-type cage. On the other hand, the integration of amide moieties on both sides, *i.e.*, **L2**, enables a family of five *cis*-$Pd_2L_2^aL_2^x$-type architectures *via* self-assembly of the conformationally adaptive ligand and complementary ligands of varied lengths ranging from 8.1 to 15 Å. Fascinatingly, adaptability of **L2** with three distinct switchable conformational states enabled us to explore the higher order 2-/3-fold heteromeric completive self-sorting. An unprecedented, cage fusion of four different homoleptic assemblies resulted in a 3-fold heteromeric completive self-sorting, where three distinct *cis*-$Pd_2L_2^aL_2^x$-type assemblies were found to co-exist in solution. The error-free orthogonality in the coordination cage system involving multiple metal–ligand interactions was a result of the ability of the conformationally adaptive ligand **L2** to attain three different conformations ($\mathbf{L2}^{SS}$, $\mathbf{L2}^{SA}$ and $\mathbf{L2}^{AA}$) in the *cis*-$Pd_2L_2^aL_2^x$-type cages. This work illustrates that the introduction of switchable conformational states in the ligand backbone paves the way for constructing new architectures with modulable cavity size, shape and functions.

## Author contributions

M. P., V. S., and D. K. C. designed the project. M. P. and V. S. carried out the research and analyzed the data. M. P., V. S., and D. K. C. wrote the manuscript. V. R. refined the SC-XRD data and contributed to the preparation of the manuscript. D. K. C. is the principal investigator and managed the project. All the authors reviewed the manuscript and have approved the final version of the manuscript.

## Conflicts of interest

There are no conflicts to declare.

## Data availability

CCDC 2466372 (**L2**) and 2466383–2466385 (**2C**·4$NO_3$, **2D**·4$NO_3$, and **2F**·4$BF_4$) contain the supplementary crystallographic data for this paper.[23a–d]

The data supporting this article have been included as part of the supplementary information (SI). Supplementary information is available. See DOI: https://doi.org/10.1039/d5sc05568g.

## Acknowledgements

D. K. C. thanks the Anusandhan National Research Foundation (ANRF) (formerly Science and Engineering Research Board (SERB)), Government of India (Project no. CRG/2022/004413), for financial support. D. K. C. thanks IIT Madras for financial support through a Mid-Career Institute Research and Development Award (Project no. IRDA-2019) and through a Center under Institute of Eminence program (IoE Center of Molecular Architecture) (Project no. IoE Phase II). M. P. thanks UGC for a fellowship. We also thank the CoE on Molecular Materials and Functions and IoE Center of Molecular Architecture for IoE funded single crystal X-ray diffraction facility. We thank the Department of Chemistry, IIT Madras, for NMR facility and DST-

 

FIST funded ESI-MS facility. We thank Ayan Ghosh, Dr. D. Elias Jesu Packiam, for rendering help in single-crystal X-ray data collection, and Dr. R. Baskar for DOSY NMR measurements. We thank the P. G. Senapathy Centre for Computing Resources, IIT Madras, for providing access to the Gaussian16 package.

## References

1 (*a*) M. Ruben, J. Rojo, F. J. Romero-Salguero, L. H. Uppadine and J.-M. Lehn, *Angew. Chem., Int. Ed.*, 2004, **43**, 3644–3662; (*b*) M. Fujita, M. Tominaga, A. Hori and B. Therrien, *Acc. Chem. Res.*, 2005, **38**, 371–380; (*c*) T. R. Cook and P. J. Stang, *Coord. Chem. Rev.*, 2015, **115**, 7001–7045; (*d*) S. D. P. Fielden, D. A. Leigh and S. L. Woltering, *Angew. Chem., Int. Ed.*, 2017, **56**, 11166–11194; (*e*) Q. Chen and K. Zhu, *Chem. Soc. Rev.*, 2024, **53**, 5677–5703; (*f*) P. J. Stang and B. Olenyuk, *Acc. Chem. Res.*, 1997, **30**, 502–518; (*g*) J. Dong, Y. Liu and Y. Cui, *Acc. Chem. Res.*, 2021, **54**, 194–206; (*h*) K. Acharyya and P. S. Mukherjee, *Angew. Chem., Int. Ed.*, 2019, **58**, 8640–8653; (*i*) J. R. Nitschke, *Acc. Chem. Res.*, 2007, **40**, 103–112; (*j*) Y.-F. Han and G.-X. Jin, *Acc. Chem. Res.*, 2014, **47**, 3571–3579.

2 (*a*) D. Zhang, T. K. Ronson, Y.-Q. Zou and J. R. Nitschke, *Nat. Rev. Chem.*, 2021, **5**, 168–182; (*b*) A. Galan and P. Ballester, *Chem. Soc. Rev.*, 2016, **45**, 1720–1737; (*c*) S. He, L. Wu, X. Li, H. Sun, T. Xiong, J. Liu, C. Huang, H. Xu, H. Sun, W. Chen, R. Gref and J. Zhang, *Acta Pharm. Sin. B*, 2021, **11**, 2362–2395; (*d*) Y. Xue, X. Hang, J. Ding, B. Li, R. Zhu, H. Pang and Q. Xu, *Coord. Chem. Rev.*, 2021, **430**, 213656; (*e*) V. Sivalingam, S. Krishnaswamy and D. K. Chand, *Chem.-Eur.J.*, 2023, **29**, e202300891.

3 A. Wu and L. Isaacs, *J. Am. Chem. Soc.*, 2003, **125**, 4831–4835.

4 (*a*) T. K. Ronson, D. A. Roberts, S. P. Black and J. R. Nitschke, *J. Am. Chem. Soc.*, 2015, **137**, 14502–14512; (*b*) Y.-R. Zheng, Z. Zhao, M. Wang, K. Ghosh, J. B. Pollock, T. R. Cook and P. J. Stang, *J. Am. Chem. Soc.*, 2010, **132**, 16873–16882; (*c*) S. Mukherjee and P. S. Mukherjee, *Chem. Commun.*, 2014, **50**, 2239–2248; (*d*) C.-B. Tian and Q.-F. Sun, *Chem.-Eur.J.*, 2023, **29**, e202300195; (*e*) J. A. Davies, T. K. Ronson and J. R. Nitschke, *J. Am. Chem. Soc.*, 2024, **146**, 5215–5223; (*f*) D. Preston and J. D. Evans, *Angew. Chem., Int. Ed.*, 2023, **62**, e202314378; (*g*) S. Pullen, J. Tessarolo and G. H. Clever, *Chem. Sci.*, 2021, **12**, 7269–7293; (*h*) Q.-F. Sun, S. Sato and M. Fujita, *Angew. Chem., Int. Ed.*, 2014, **53**, 13510–13513; (*i*) S. Sudan, R.-J. Li, S. M. Jansze, A. Platzek, R. Rudolf, G. H. Clever, F. Fadaei-Tirani, R. Scopelliti and K. Severin, *J. Am. Chem. Soc.*, 2021, **143**, 1773–1778; (*j*) S. Prusty, K. Yazaki, M. Yoshizawa and D. K. Chand, *Chem.-Eur.J.*, 2017, **23**, 12456–12461; (*k*) S. Samantray, S. Krishnaswamy and D. K. Chand, *Nat. Commun.*, 2020, **11**, 880.

5 (*a*) D. A. McMorran and P. J. Steel, *Angew. Chem., Int. Ed.*, 1998, **37**, 3295–3297; (*b*) W. M. Bloch, J. J. Holstein, W. Hiller and G. H. Clever, *Angew. Chem., Int. Ed.*, 2017, **56**, 8285–8289; (*c*) Y. Liu, S.-H. Liao, W.-T. Dai, Q. Bai, S. Lu, H. Wang, X. Li, Z. Zhang, P. Wang, W. Lu and Q. Zhang, *Angew. Chem., Int. Ed.*, 2023, **62**, e202217215; (*d*) T. Abe, N. Sanada, K. Takeuchi, A. Okazawa and S. Hiraoka, *J. Am. Chem. Soc.*, 2023, **145**, 28061–28074; (*e*) K. Wu, E. Benchimol, A. Baksi and G. H. Clever, *Nat. Chem.*, 2024, **16**, 584–591.

6 M. L. Saha, S. De, S. Pramanik and M. Schimttel, *Chem. Soc. Rev.*, 2013, **42**, 6860–6909.

7 E. Benchimol, I. Regeni, B. Zhong, M. Kabiri, J. J. Holstein and G. H. Clever, *J. Am. Chem. Soc.*, 2024, **146**, 6905–6911.

8 M. Parbin, V. Sivalingam and D. K. Chand, *Angew. Chem., Int. Ed.*, 2024, **63**, e202410219.

9 M. L. Saha and M. Schmittel, *Org. Biomol. Chem.*, 2012, **10**, 4651–4684.

10 (*a*) T. Haliloglu and I. Bahar, *Curr. Opin. Struct. Biol.*, 2015, **35**, 17–23; (*b*) S. Corless and N. Gilbert, *Biophys. Rev.*, 2016, **8**, 245–258; (*c*) S. Raman, *Biochemistry*, 2018, **57**, 376–382.

11 (*a*) Y.-H. Huang, Y.-L. Lu, J. Ruan, S.-P. Zheng, X.-D. Zhang, C.-H. Liu, Y.-H. Qin, Z.-M. Cao, Z. Jiao, H.-S. Xu and C.-Y. Su, *J. Am. Chem. Soc.*, 2023, **145**, 23361–23371; (*b*) D. Zhang, Q. Gan, A. J. Plajer, R. Lavendomme, T. K. Ronson, Z. Lu, J. D. Jensen, B. W. Laursen and J. R. Nitschke, *J. Am. Chem. Soc.*, 2022, **144**, 1106–1112; (*c*) J. Mendez-Arroyo, J. Barroso-Flores, A. M. Lifschitz, A. A. Sarjeant, C. L. Stern and C. A. Mirkin, *J. Am. Chem. Soc.*, 2014, **136**, 10340–10348; (*d*) A. P. Gia, A. de. Juan, D. Aranda, F. G. Guijarro, J. Aragó, E. Ortí, M. García-Iglesias and D. González-Rodríguez, *J. Am. Chem. Soc.*, 2025, **147**, 918–931; (*e*) H. Xu, T. K. Ronson, A. W. Heard, P. C. P. Teeuwen, L. Schneider, P. Pracht, J. D. Thoburn, D. J. Wales and J. R. Nitschke, *Nat. Chem.*, 2025, **17**, 289–296; (*f*) W. L. Jiang, B. Huang, X. L. Zhao, X. Shi and H. B. Yang, *Chem*, 2023, **9**, 2655–2668; (*g*) J. Mosquera, T. K. Ronson and J. R. Nitschke, *J. Am. Chem. Soc.*, 2016, **138**, 1812–1815.

12 (*a*) R. Yamasaki, A. Tanatani, I. Azumaya, S. Saito, K. Yamaguchi and H. Kagechika, *Org. Lett.*, 2003, **5**, 1265–1267; (*b*) J. K. R. Deka, B. Sahariah, K. Baruah, A. K. Bar and B. K. Sarma, *Chem. Commun.*, 2020, **56**, 4874–4877; (*c*) P. Xing, Y. Liu, B. Li, Z.-Y. Dong, H.-J. Qian and L. Wang, *Inorg. Chim. Acta.*, 2022, **536**, 120854.

13 (*a*) W. M. Bloch, Y. Abe, J. J. Holstein, C. M. Wandtke, B. Dittrich and G. H. Clever, *J. Am. Chem. Soc.*, 2016, **138**, 13750–13755; (*b*) A. Platzek, S. Juber, C. Yurtseven, S. Hasegawa, L. Schneider, C. Drechsler, K. E. Ebbert, R. Rudolf, Q.-Q. Yan, J. J. Holstein, L. V. Schafer and G. H. Clever, *Angew. Chem., Int. Ed.*, 2022, **61**, e202209305.

14 R. S. Rarig, R. Lam, P. Y. Zavalij, J. K. Ngala, R. L. LaDuca, J. E. Greedan and J. Zubieta, *Inorg. Chem.*, 2002, **41**, 2124–2133.

15 E. Bosch and C. L. Barnes, *New J. Chem.*, 2001, **25**, 1376–1378.

16 D. K. Chand, K. Biradha, M. Kawano, S. Sakamoto, K. Yamaguchi and M. Fujita, *Chem.–Asian J.*, 2006, **1**, 82–90.

17 E. Merkul, D. Urselmann and T. J. J. Müller, *Eur. J. Org Chem.*, 2011, **2011**, 238–242.

18 K. J. Kilpin, M. L. Gower, S. G. Telfer, G. B. Jameson and J. D. Crowley, *Inorg. Chem.*, 2011, **50**, 1123–1134.

19 H. Yu, Z. Guo, J. Tang, N. Han, J. Shi, M. Li, H. Zhang and M. Wang, *Chem. Sci.*, 2025, **16**, 6114–6120.

20 R.-J. Li, J. de Montmollin, F. Fadaei-Tirani, R. Scopelliti and K. Severin, *Dalton Trans.*, 2023, **52**, 6451–6456.
21 J. A. Findlay, K. M. Patil, M. G. Gardiner, H. I. MacDermott-Opeskin, M. L. O'Mara, P. E. Kruger and D. Preston, *Chem.–Asian J.*, 2022, **17**, e202200093.
22 A. Tarzia, W. Shan, V. Posligua, C. J. T. Cox, L. Male, B. D. Egleston, R. L. Greenaway, K. E. Jelfs and J. E. M. Lewis, *Chem.-Eur.J.*, 2025, **31**, e202403336.
23 (*a*) CCDC 2466372: Experimental Crystal Structure Determination, 2025, DOI: 10.5517/ccdc.csd.cc2nsgdb; (*b*) CCDC 2466383: Experimental Crystal Structure Determination, 2025, DOI: 10.5517/ccdc.csd.cc2nsgrp; (*c*) CCDC 2466384: Experimental Crystal Structure Determination, 2025, DOI: 10.5517/ccdc.csd.cc2nsgsq; (*d*) CCDC 2466385: Experimental Crystal Structure Determination, 2025, DOI: 10.5517/ccdc.csd.cc2nsgtr.